**ELECTRONIC SUPPLEMENTARY INFORMATION (ESI) FOR:**

# Sterically Demanding Methoxy and Methyl Groups in Ruthenium Complexes Lead to Enhanced Quantum Yields for Blue Light Triggered Photodissociation

*Fengrui Qu,[a] Kristina Martinez,[b] Ashley M. Arcidiacono,[c] Seungjo Park,[d] Matthias Zeller,[e] Russell H. Schmehl,[b] Jared J. Paul,*[,c] Yonghyun Kim,*[,d] Elizabeth T. Papish*[,a]*

[a]*Department of Chemistry, The University of Alabama, Tuscaloosa, AL 35487-0336, USA. E-mail: etpapish@ua.edu.*
[b]*Department of Chemistry, Tulane University, New Orleans, Louisiana 70118, United States*
[c]*Department of Chemistry, Villanova University, Villanova, PA 19085, USA. E-mail: jared.paul@villanova.edu.*
[d]*Department of Chemical and Biological Engineering, The University of Alabama, Tuscaloosa, AL 35487-0203, USA. E-mail: ykim@eng.ua.edu.*
[e]*Department of Chemistry, Purdue University, West Lafayette, IN 47907, USA*

Table of Contents

## I. General specifications

All experiments were carried out under a nitrogen atmosphere using glovebox or standard Schlenk techniques if not indicated otherwise. All reagents for which synthesis is not given were commercially available from Sigma-Aldrich, Acros, Strem or Pressure Chemical and were used as received without further purification. Solvents were purified prior to use by passing through a column of activated alumina using a Glass Contour Solvent Purification System. $^{1}H$, $^{13}C$-NMR spectra were acquired at room temperature on a Bruker AV360 360 MHz or AV500 500 MHz spectrometer, as designated. Chemical shifts are reported in ppm and referenced to TMS (if available) or residual solvent resonance peaks. Abbreviations for the multiplicity of NMR signals are s (singlet), d (doublet), t (triplet), q (quartet), m (multiplet) and br (broad). UV-Visible spectra were recorded on a Perkin Elmer Lambda 35 UV-Visible spectrometer. Mass spectrometric data were collected on a Waters AutoSpec-Ultima NT spectrometer with electron ionization method. ESI mass-spectrometry was provided by the University of Alabama Mass Spectrometry Resource. Elemental analyses were performed by Atlantic Microlab, Inc., Norcross, GA.

## II. NMR spectra.

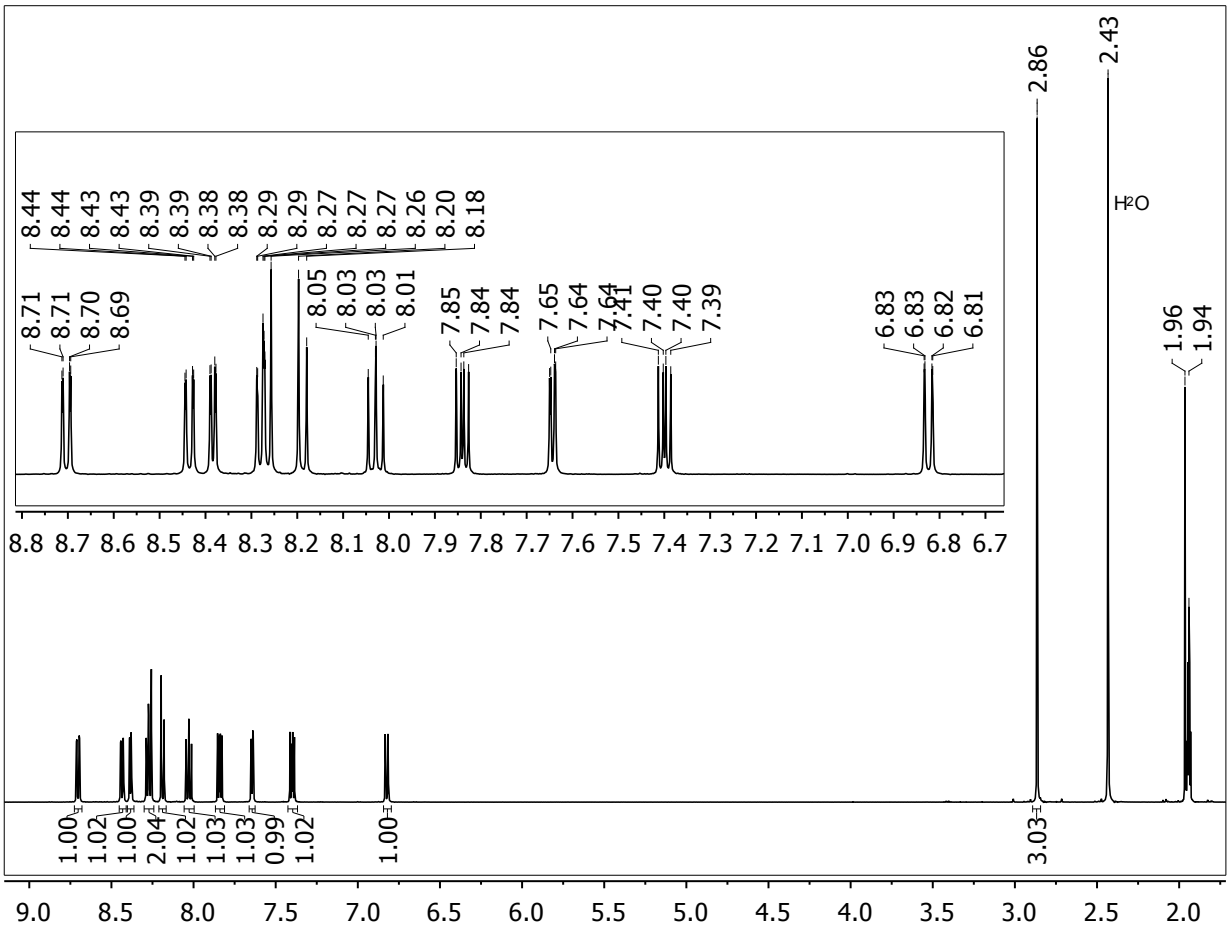


Figure S1 – $^{1}$H NMR of **2$^{OMe}$**: $[(phen)_2Ru(6,6'\text{-dmbp})]Cl_2$ in $CD_3CN$.

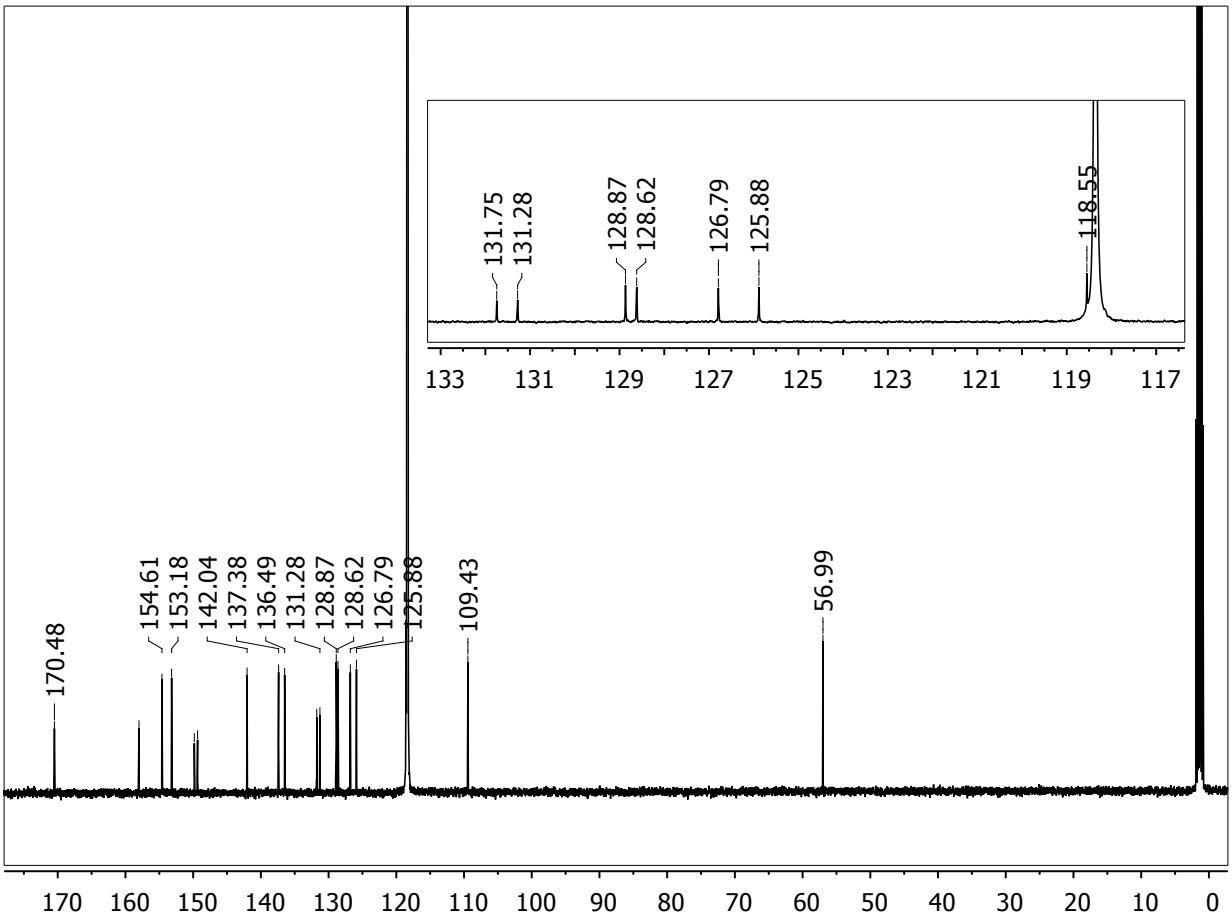


Figure S2 – $^{13}C$ NMR of **2**$^{\mathbf{OMe}}$: $[(phen)_2Ru(6,6'\text{-dmbp})]Cl_2$ in $CD_3CN$.

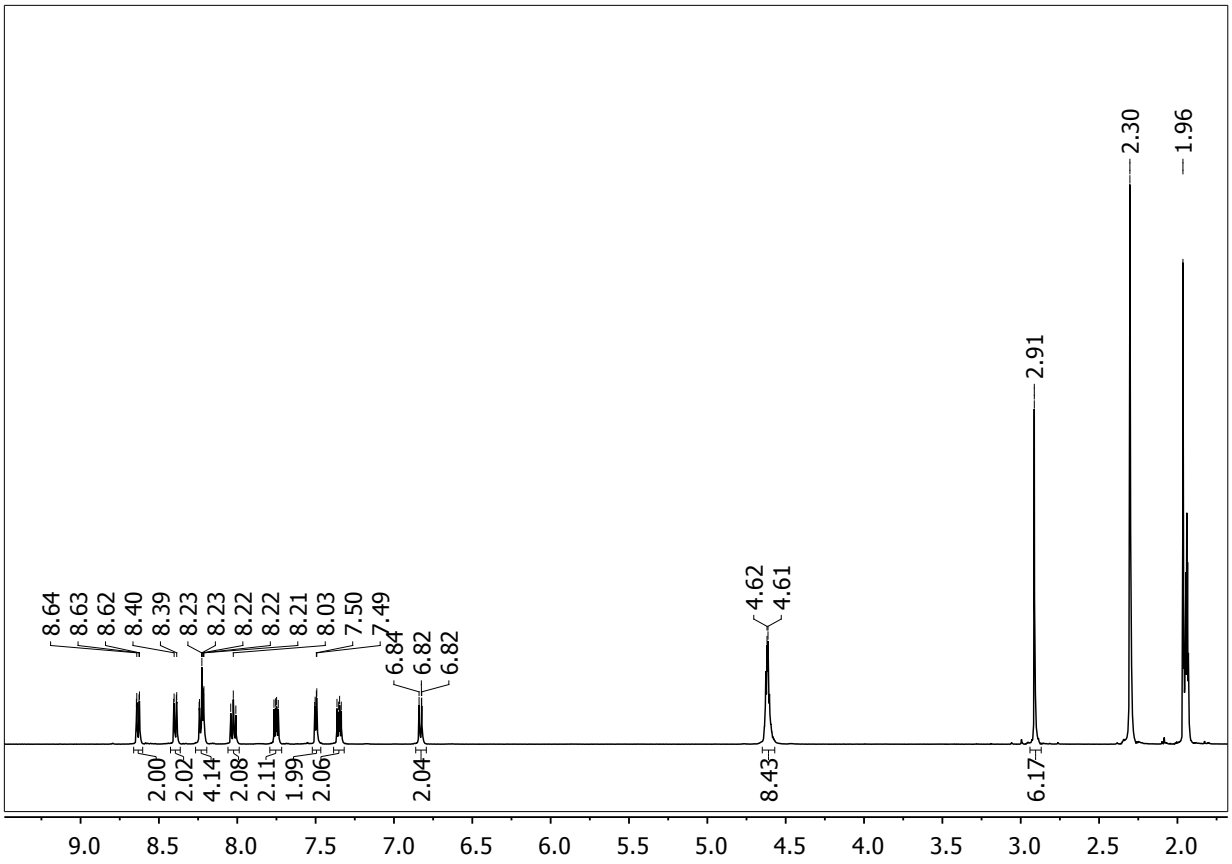


Figure S3 – $^{1}H$ NMR of $\mathbf{3}^{\mathbf{OMe}}$: $[(dop)_2Ru(6,6'\text{-}dmbp)]Cl_2$ in $CD_3CN$.

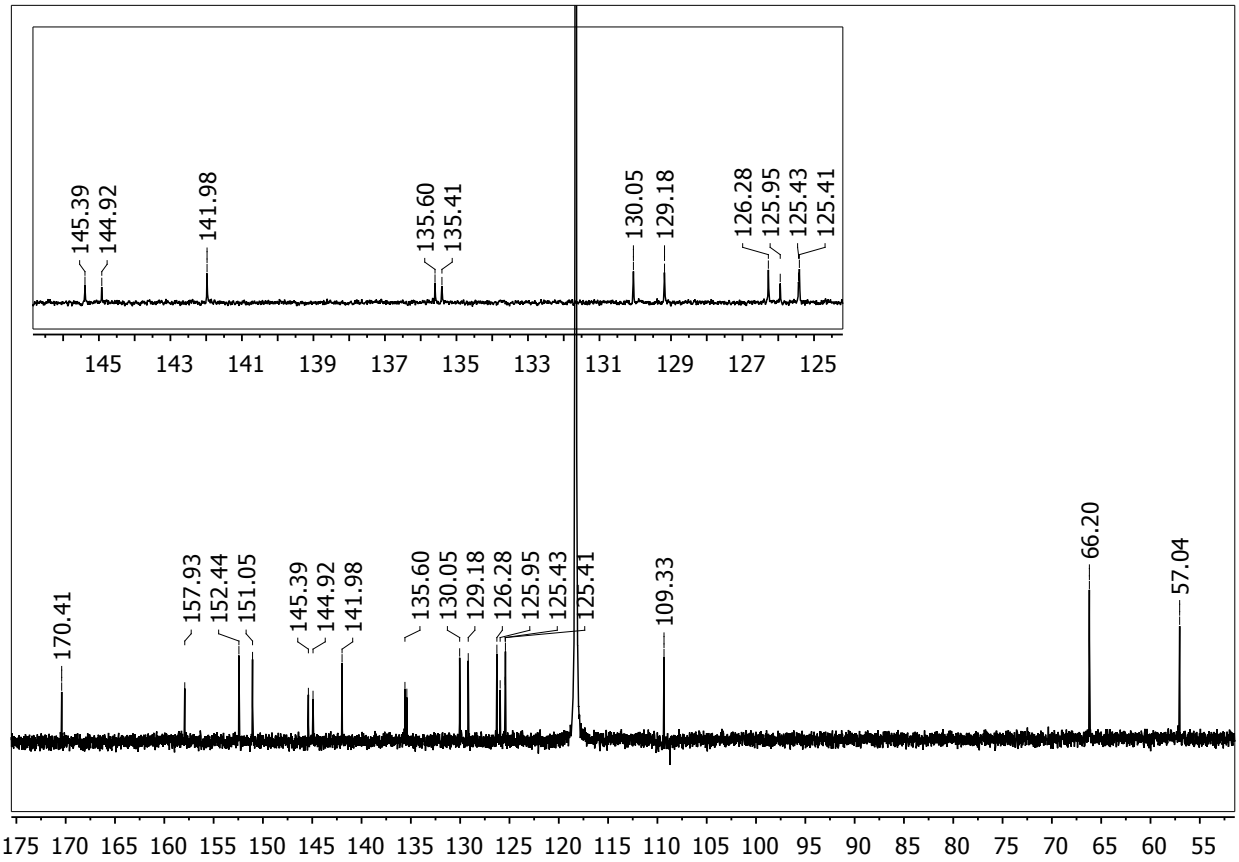


Figure S4 – $^{13}C$ NMR of $\mathbf{3^{OMe}}$: $[(dop)_2Ru(6,6'\text{-}dmbp)]Cl_2$ in $CD_3CN$.

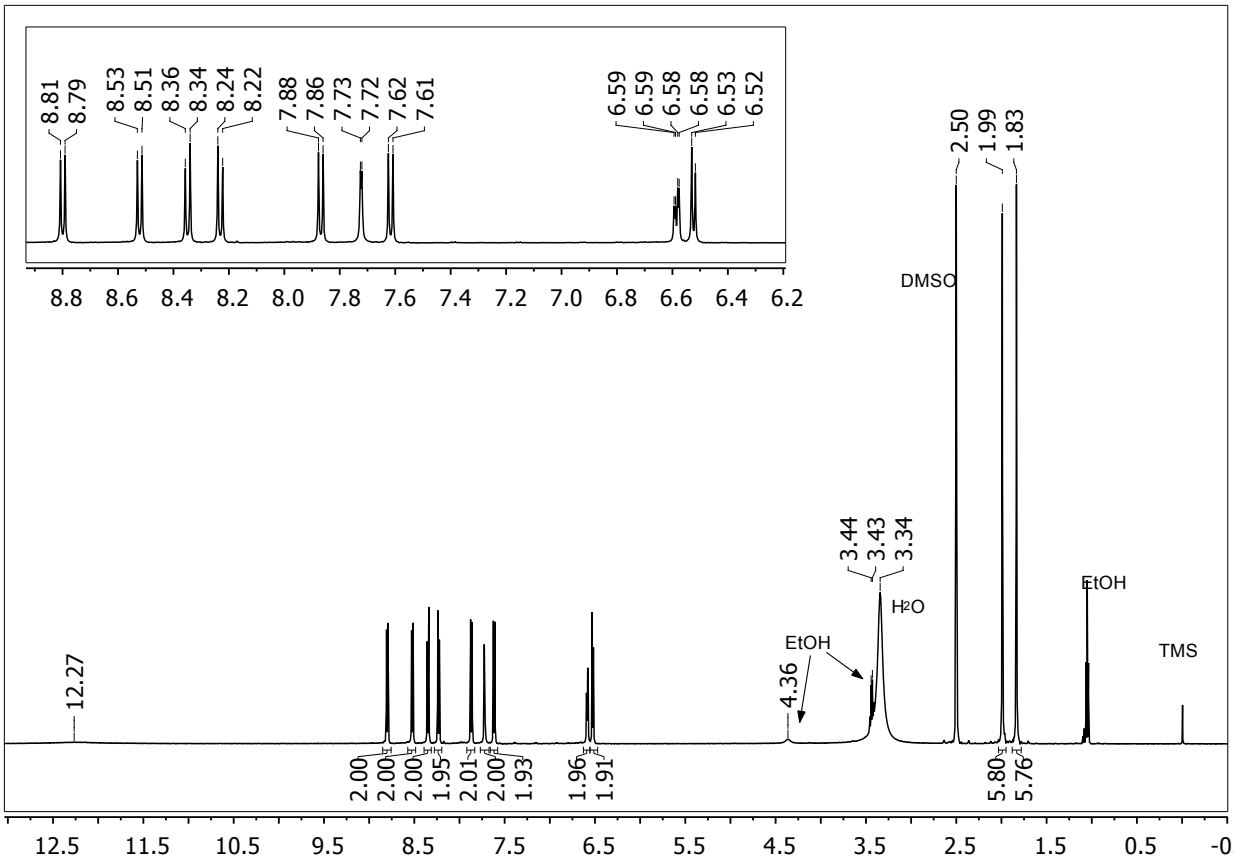


Figure S5 – $^{1}H$ NMR of $\mathbf{4^{OH}}$: $[(neo)_2Ru(4,4'\text{-}dhbp)]Cl_2$ in DMSO-$d^6$.

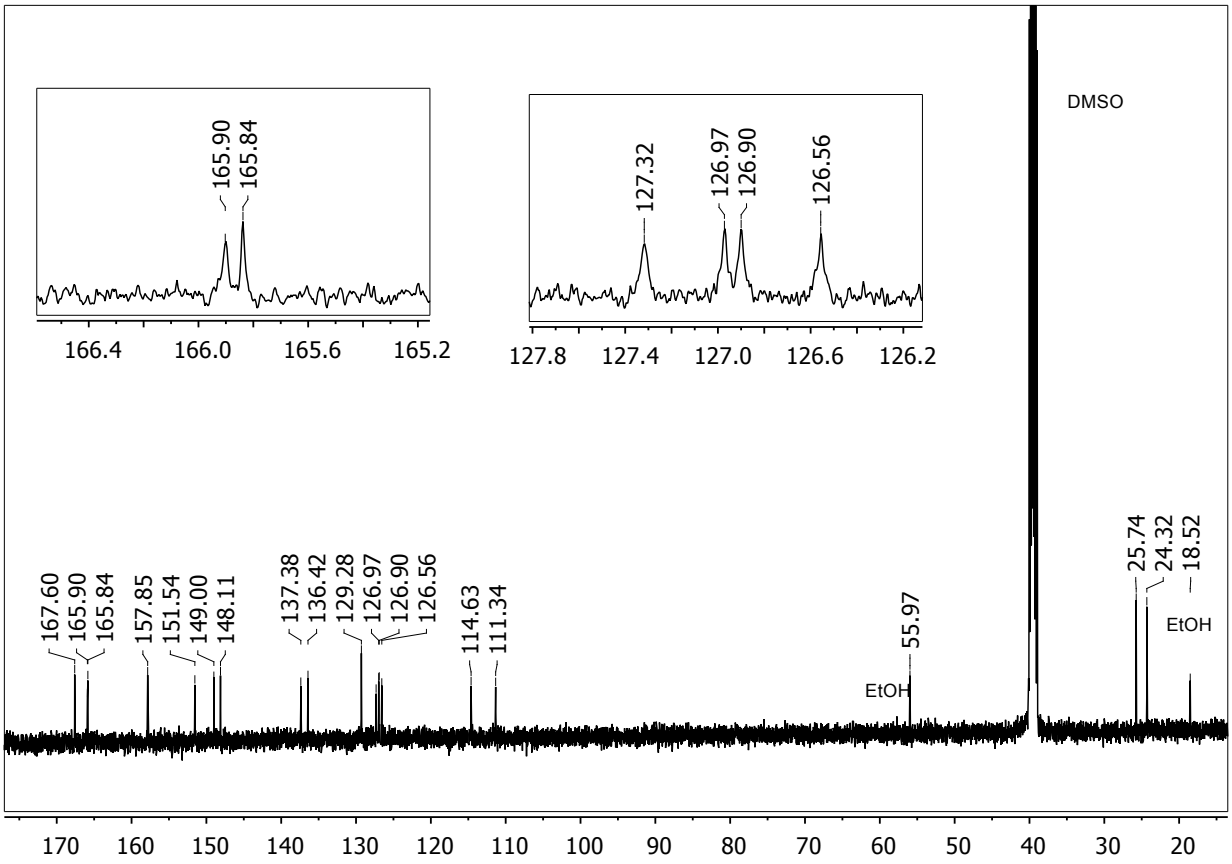


Figure S6 – $^{13}C$ NMR of **4$^{OH}$**: $[(neo)_2Ru(4,4'\text{-bp})]Cl_2$ in DMSO-$d^6$.

## III. UV-Vis spectra of $2^{OMe}$, $3^{OMe}$ and $4^{OH}$ in DI water.

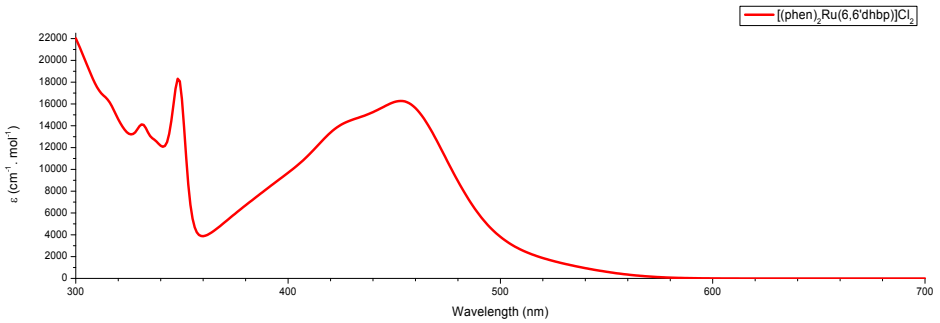


Figure S7 – UV-Vis spectrum of $\mathbf{2^{OMe}}$ in DI water.

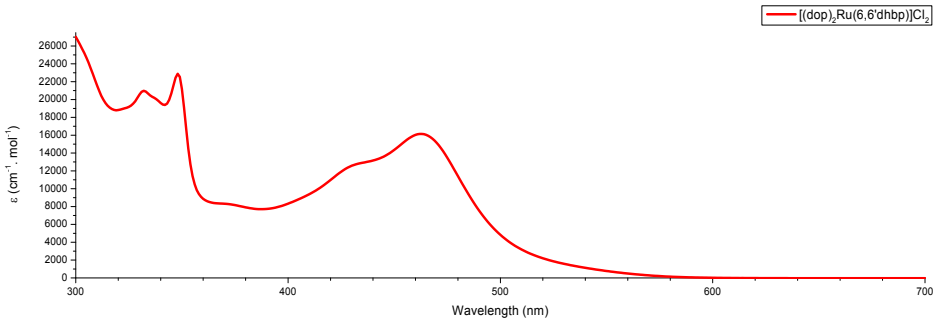


Figure S8 – UV-Vis spectrum of $\mathbf{3^{OMe}}$ in DI water.

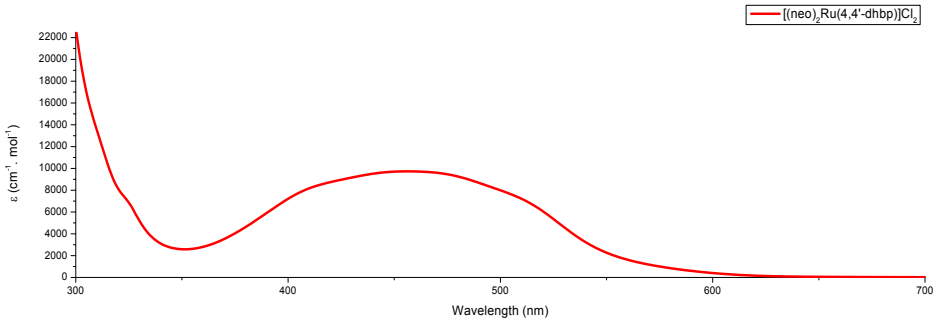


Figure S9 – UV-Vis spectrum of $\mathbf{4^{OH}}$ in DI water.

## IV. p$K_a$ determination for $4^{OH}$.

### p$K_a$ by potentiometric titration.

An aqueous solution of the analyte compound was pre-treated with 4 eq of HCl to make sure the compound was doubly protonated. The solution was titrated with dilute standardized NaOH solution in dark room. The pH vs volume of the NaOH solution was plotted and the first derivative was taken, which was used to derive the p$K_a$ value. The experiments were repeated 3 times to determine an average value. It was found that only one p$K_a$ value was obtained in this way, which was assigned as the average p$K_a$ for the diprotic compound/diacid.

Table S1 - p$K_a$ determination for **$4^{OH}$** by potentiometric method.

| Compound | Trial 1 | Trial 2 | Trial 3 | Average |
|---|---|---|---|---|
| $[(neo)_2Ru(4,4'\text{-}dhbp)]Cl_2$, **$4^{OH}$** | 6.10 | 6.08 | 6.07 | 6.08(2) |

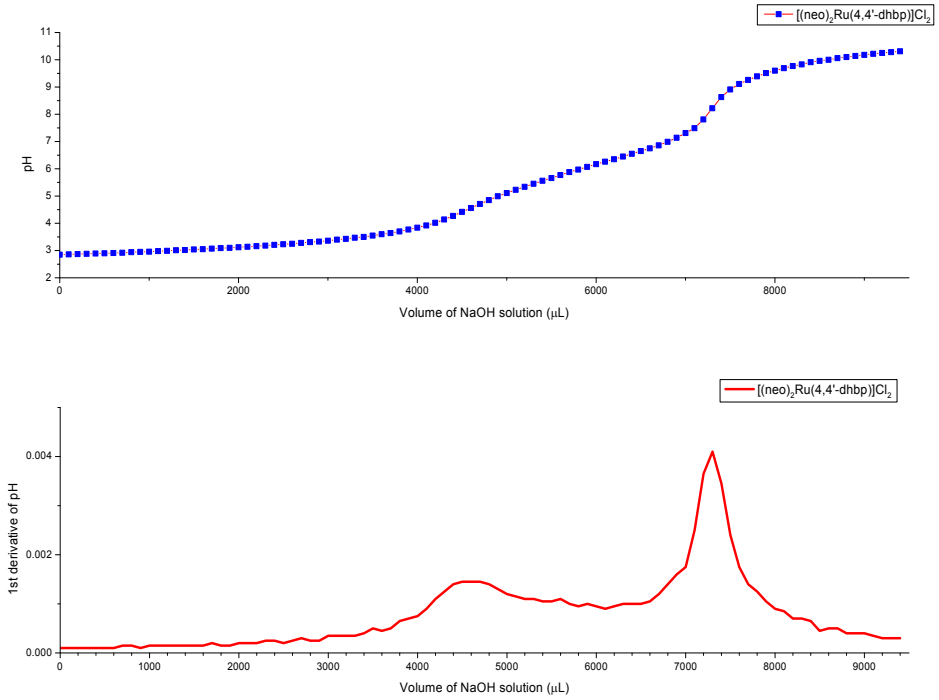


Figure S10 – p$K_a$ determination for **$4^{OH}$** by potentiometric titration. Top: Titration curve of **$4^{OH}$** by aqueous NaOH solution. Bottom: 1st derivative of the titration curve, showing two distinctive peaks.

## V. IR of $2^{OMe}$, $3^{OMe}$ and $4^{OH}$.

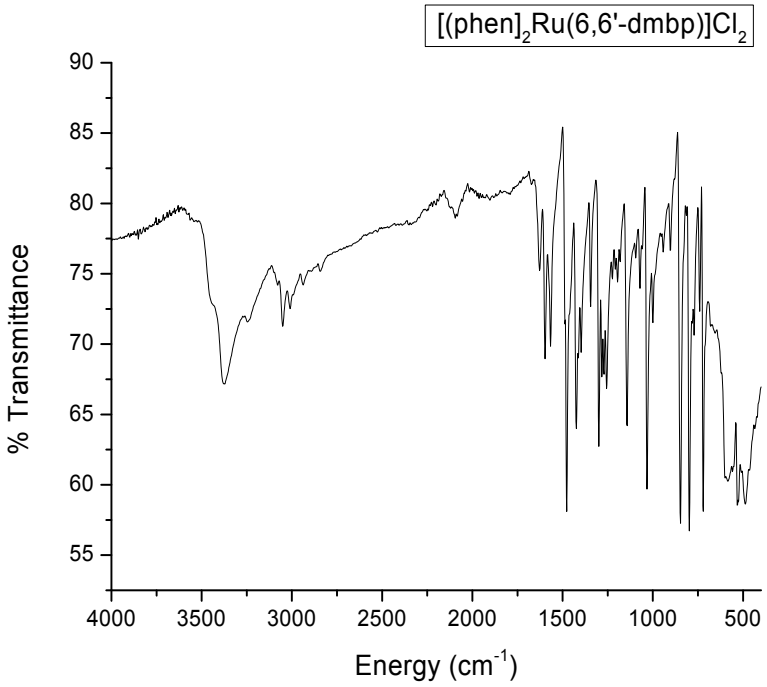


Figure S11 – FT-IR spectrum of of $\mathbf{2^{OMe}}$.

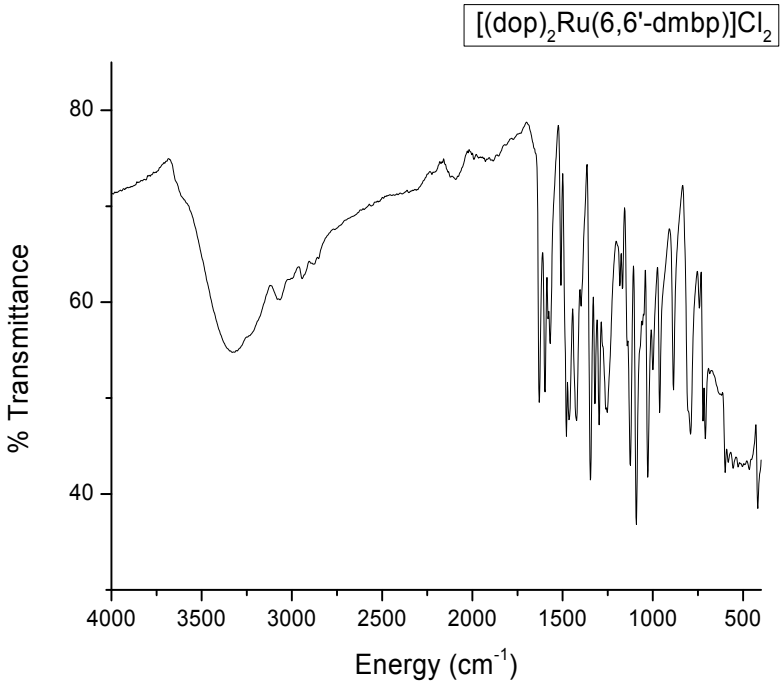


Figure S12 – FT-IR spectrum of of $\mathbf{3^{OMe}}$.

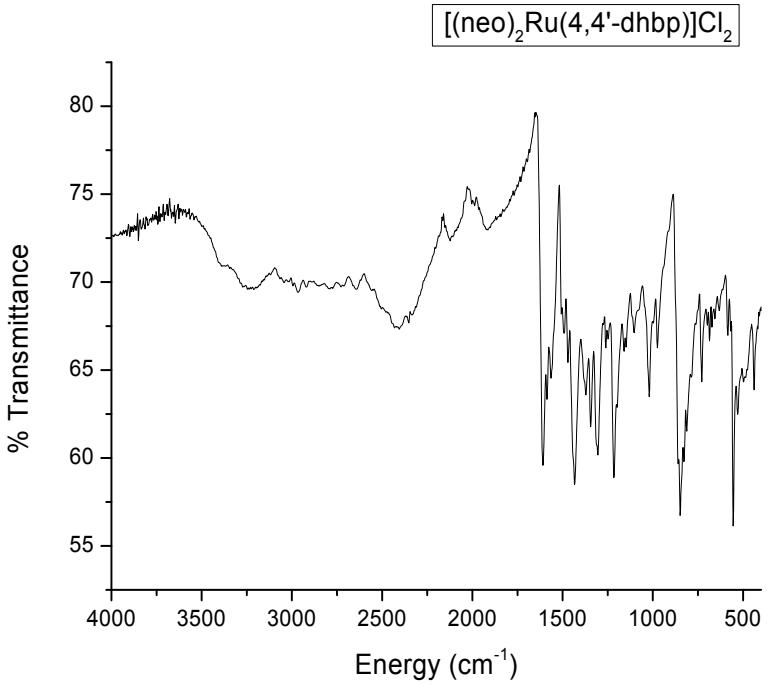


Figure S13 – FT-IR spectrum of $\mathbf{4^{OH}}$.

VI. **Determination of Log $D_{7.40}$** (Octanol/Water) for **$2^{OMe}$**, **$3^{OMe}$** and **$4^{OH}$**.

General procedure for the determination of Log $D_{7.40}$:

The solution was protected from light throughout the experimental procedure. A 25 mL of the octanol stock solution of the target complex was prepared by dissolving known amount of the Ru complex into 25 mL of octanol. 1mL of the Ru stock solution was diluted by 3 mL of fresh octanol, followed by 4 mL of pH 7.4 phosphate buffer (*aq*.). The final solution was left to stir for 24 hrs at room temperature in dark. The two phases were then separated and serial dilutions were prepared and analyzed via UV-Vis spectroscopy (700 nm-300 nm) to determine the concentration of the ruthenium complex in solution. Log $D_{7.40}$ was calculated by the following equation: $Log(D) = [Ru]_{octanol} / [Ru]_{aqueous}$. The result was summarized in the following table.

Table S2. LogD determination for **$2^{OMe}$**, **$3^{OMe}$** and **$4^{OH}$**.

| Complexes | pH | logD-trial 1 | Trial 2 | Trial 3 | Ave. |
|---|---|---|---|---|---|
| **$2^{OMe}$** | 7.4 | -1.106 | -1.283 | -1.498 | -1.3(2) |
| **$3^{OMe}$** | 7.4 | -1.089 | -1.123 | -1.091 | -1.10(2) |
| **$4^{OH}$** | 7.4 | 0.598 | 0.587 | 0.564 | 0.58(2) |

## VII. Cyclic Voltammetry study of $2^{OMe}$, $3^{OMe}$ and $4^{OH}$.

*Buffer System for Electrochemical pH Studies*

pH measurements were carried out using a VWR SympHony pH meter, utilizing a three-point calibration at pH = 4, 7, and 10. Britton-Robinson buffer solutions were made from a stock solution of 0.04 M acetic acid, 0.04 M boric acid, and 0.04 M phosphoric acid with the addition of 0.2 M sodium hydroxide to achieve an approximate pH of 7 for the solution after the addition of the metal complex.[1]

*Cyclic Voltammetry*

Cyclic voltammetry measurements were performed on a Bioanalytical Systems CW-50 potentiostat. Typical concentrations for metal complexes ranged from 0.64 to 0.84 mM. Studies were carried out in aqueous Britton-Robinson buffer solutions as the supporting electrolyte. The pH of each solution was checked after the dissolution of metal complex for study. A three electrode setup with an Ag/AgCl reference electrode, platinum wire auxiliary electrode, and glassy carbon working electrode was used. In all studies, the solutions were degassed for approximately 30 minutes with argon prior to data collection and the glassy carbon electrode was polished before each scan.

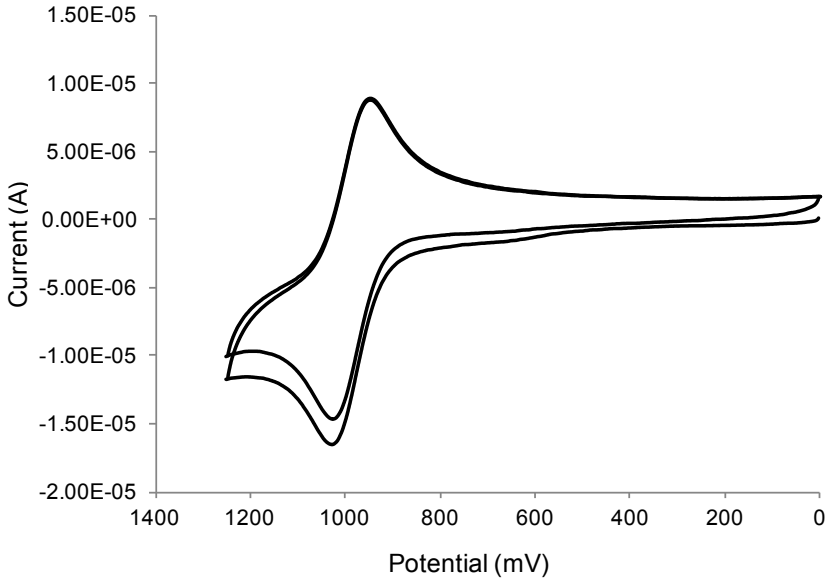


Figure S14 – Cyclic voltammogram (oxidative scan) of 0.84 mM $\mathbf{2^{OMe}}$ in Britton-Robinson supporting electrolyte at pH = 7.0 with glassy carbon working electrode at 25 °C. Scan rate was 200 mV/s. Potentials are reported vs. Ag/AgCl.

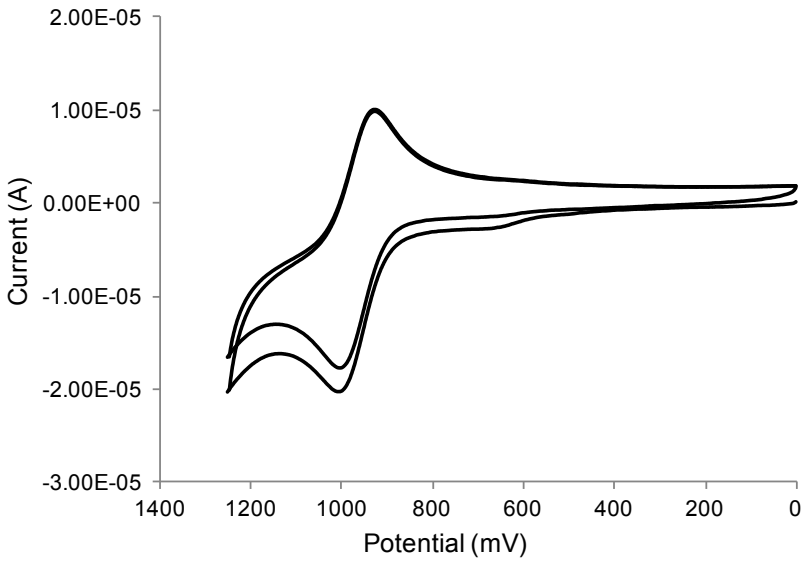


Figure S15 – Cyclic voltammogram (oxidative scan) of 0.81 mM **3**$^{OMe}$ in Britton-Robinson supporting electrolyte at pH = 7.0 with glassy carbon working electrode at 25 °C. Scan rate was 200 mV/s. Potentials are reported vs. Ag/AgCl.

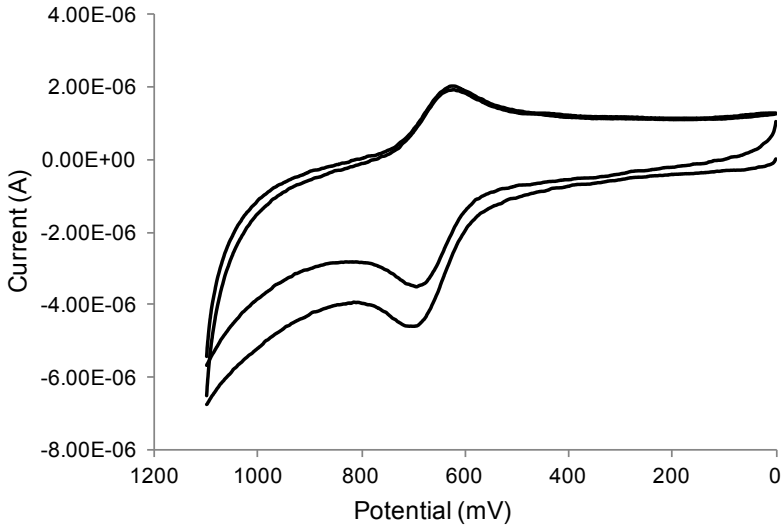


Figure S16 – Cyclic voltammogram (oxidative scan) of 0.64 mM **4**$^{OH}$ in Britton-Robinson supporting electrolyte at pH = 7.0 with glassy carbon working electrode at 25 °C. Scan rate was 200 mV/s. Potentials are reported vs. Ag/AgCl.

Table S3. $Ru^{II/III}$ redox potentials of $\mathbf{2}^{\mathbf{OMe}}$, $\mathbf{3}^{\mathbf{OMe}}$ and $\mathbf{4}^{\mathbf{OH}}$ at varying scan rate.

| Complexes | Scan Rate (mV/s) | $E_{1/2}$ $Ru^{III/II}$ vs. Ag/AgCl(V) |
|---|---|---|
| $\mathbf{2}^{\mathbf{OMe}}$ | 50 | 0.99 |
| | 100 | 0.99 |
| | 200 | 0.99 |
| | 300 | 0.99 |
| | 400 | 0.99 |
| | 500 | 0.99 |
| | 1000 | 0.99 |
| $\mathbf{3}^{\mathbf{OMe}}$ | 50 | 0.98 |
| | 100 | 0.98 |
| | 200 | 0.98 |
| | 300 | 0.97 |
| | 400 | 0.98 |
| | 500 | 0.97 |
| | 1000 | 0.98 |
| $\mathbf{4}^{\mathbf{OH}}$ | 50 | 0.66 |
| | 100 | 0.66 |
| | 200 | 0.66 |
| | 300 | 0.66 |
| | 400 | 0.66 |
| | 500 | 0.67 |
| | 1000 | 0.67 |

## VIII. Quantum yield study of $2^{OMe}$, $3^{OMe}$ and $4^{OH}$

*Instrumentation:*

A PTI Felix 32TM MD-5020 spectrofluorimeter was used for all experiments. The slit widths were set to 4 mm. The wavelength was set to 451 nm. Absorption spectra were acquired on a Hewlett Packard 8452 diode array spectrophotometer.

*Preparation of Solutions:*

Two solutions were prepared for actinometry. A solution of potassium ferrioxalate was prepared by dissolving 3.7023 g (0.1507 M) of potassium ferrioxalate in a 50 mL 0.05 M $H_2SO_4$ solution. The second solution prepared was a 0.1% 1,10-phenanthroline solution in buffer. To prepare this solution, 56.25 g of sodium acetate trihydrate, 250 mg 1,10-phenanthroline, and 7 mL of $H_2SO_4$ was combined in a 250 mL volumetric flask and diluted with DI water.

*Measurement:*

A 3 mL aliquot of $K_3[Fe(C_2O_4)_3]$ was irradiated for a duration of time. An identical sample was also prepared and maintained in the dark. Following irradiation, 0.5 mL of buffered 1,10-phenanthroline solution were added to the sample, and an absorption spectrum was collected. The following table includes shows each trial and the resulting absorbance at 510 nm.

Table S4.

| **Irradiation Time (sec)** | **Absorbance @ 510 nm** | **$[Fe(phen)_3]^{2+}$** |
|---|---|---|
| 0 | 0.04774 | 4.3009E-6 |
| 10 | 0.26122 | 2.35333E-5 |
| 10 | 0.24896 | 2.24288E-5 |
| 20 | 0.47163 | 4.24892E-5 |
| 20 | 0.3344 | 3.01261E-5 |
| 30 | 0.64478 | 5.80883E-5 |
| 30 | 0.629 | 5.66667E-5 |
| 40 | 0.83307 | 7.50514E-5 |
| 40 | 0.86261 | 7.77126E-5 |
| 60 | 1.22636 | 1.10483E-4 |

*Analysis:* The following equation was used to determine the number of moles of ferrous ions formed during irradiation:

$$Moles\ Fe^{2+} = \frac{V_1 \times V_3 \times \Delta A(510nm)}{10^3 \times V_2 \times l \times \varepsilon(510nm)}$$

Where $V_1$ is the volume of ferrioxalate irradiated, $V_2$ is the aliquot of irradiated solution taken to determine $[Fe^{2+}]$, $V_3$ is the volume after complexation with 1,10-phenanthroline, $l$ is the path length, $\Delta A$ is the difference in absorbance between the irradiated solution and the solution kept in the dark, $\varepsilon$ is the molar absorptivity of $[Fe(phen)_3]^{2+}$.

The following table shows the moles of ferrous ions for each irradiation time:

Table S5.

| **Irradiation Time (sec)** | **Moles of $Fe^{2+}$** |
|---|---|
| 10 | 6.73135E-9 |
| 10 | 6.34477E-9 |
| 20 | 1.33659E-8 |
| 20 | 9.03883E-9 |
| 30 | 1.88256E-8 |
| 30 | 1.8328E-8 |
| 40 | 2.47627E-8 |
| 40 | 2.56941E-8 |
| 60 | 3.71637E-8 |

To determine the photon flux, the following equation was used:

$$\frac{Nh\nu}{t} = \frac{moles\ of Fe^{2+}}{\varphi_{451nm} \times t \times F}$$

Where $\varphi_{451nm}$ is the quantum yield of ferrous ions at 451 nm (0.96), $t$ is the irradiation time, and $F$ is the fraction of light absorbed. The fraction of light absorbed by the actinometer solution was calculated to be 98.05% or 0.9805. [We used 98% light absorbed for two reasons. The first is that the quantum yield for the formation of Fe(II) by irradiation is reported for a specific concentration of potassium ferrioxalate at the wavelength for which the photon flux was measured. Given the concentration, the absorbance value was determined at the irradiation wavelength and the fraction of light absorbed was calculated to be 98%. The second reason for the fraction of light absorbed being close to 100% is because in order to measure the moles of photons per unit time that are emitted from our light source, it is important to keep the fraction of light absorbed by the sample as uniform as possible through the irradiation time, as consumption of the Fe(III) in solution changes the absorbance at the exciting wavelength of light. The ferrioxalate concentration and absorbance change negligibly during the time of photolysis in the quantum yield measurement.]

The photon flux measured for each irradiation time are shown in the table below:

Table S6.

| **Irradiation Time (sec)** | **Photon Flux (Einstein/Minute)** |
|---|---|
| 10 | 4.29076E-08 |
| 10 | 4.04435E-08 |
| 20 | 4.25991E-08 |
| 20 | 2.88081E-08 |
| 30 | 0.00000004 |
| 30 | 3.89427E-08 |
| 40 | 3.94612E-08 |
| 40 | 4.09455E-08 |
| 60 | 3.94821E-08 |

Actinometry was repeated for a second time to verify the photon flux. Results agreed with originally measured photon flux.

**Quantum Yield Measurements:**

All measurements were carried out in a buffered phosphate solution with a concentration of 0.01 M and a pH of 5.1. Before measuring the quantum yield, steady-state photolysis was carried out over a period of several hours. The results are shown in the figure below.

**$2^{OMe}$:**

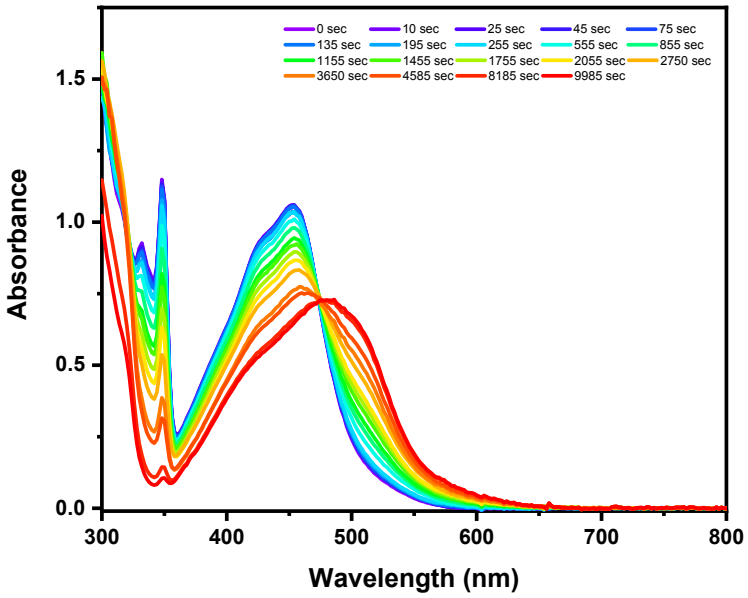


Figure S17. Steady state photolysis of **$2^{OMe}$** in buffered phosphate solution over several hours.

Upon ligand loss, the spectrum red shifts. After photolysis, a mass spectrum was collected by ESI-MS, shown in the figure below. The bottom mass spectrum is representative of the calculated spectrum for the complex **$2^{OMe}$**, while the top spectrum is from the photoproduct after irradiating for approximately 2 hours and 45 minutes.

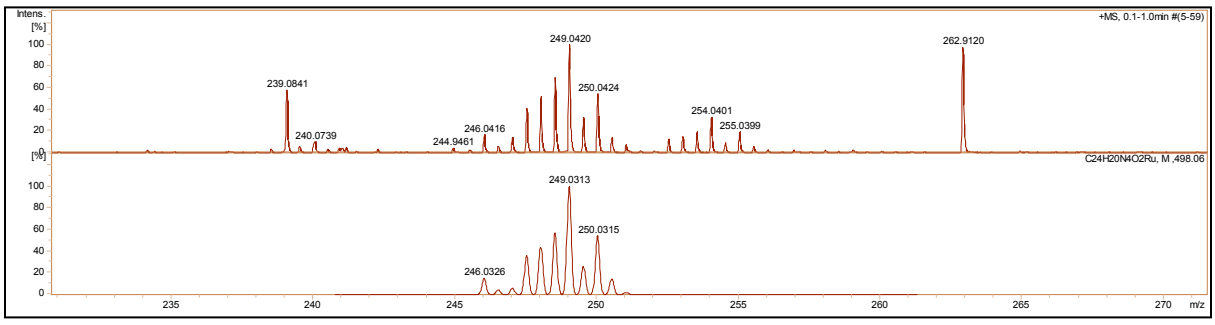

Figure S18. ESI-MS spectrum of the post-photolysis sample.

The molar absorptivity at 450 nm was determined from the slope of the linear fit from the graph below, divided by the path length of the cell, 1 cm. The molar absorptivity at 450 nm is 15066 $M^{-1}cm^{-1}$.

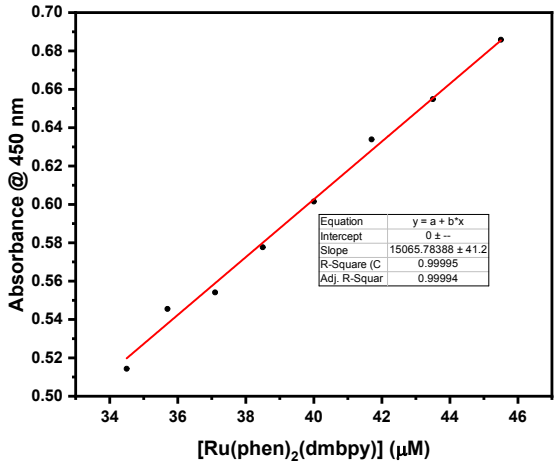


Figure S19. Molar absorptivity determination of $\mathbf{2}^{\mathbf{OMe}}$ at 450 nm.

For quantum yield calculations, the change in absorbance at 450 nm was observed with a less than 10% change in A. The relationship between the absorbance of the starting ruthenium complex and photoproduct is shown in the following equation:

$$A_{450\,nm} = A_R + A_P = \varepsilon_R l[R] + \varepsilon_P l[P]$$

If the concentration of the photoproduct is less than 10%, it can be assumed to have a small impact on the overall absorbance at 450 nm. This approach was used to calculate the quantum yield for the complex examined in this work.

For each photolysis performed, a sample was prepared in a 1 cm path length cuvette using 2 mL of known concentration solution in 0.01 M phosphate buffer with a pH of 5.1. Each sample was irradiated for a total of 10 minutes, while absorbance spectra were collected every 30 seconds for the first 5 minutes and every minute thereafter. A series of four iterations for the photolysis were conducted. The following spectra show the change in absorbance with irradiation time for each of the four iterations.

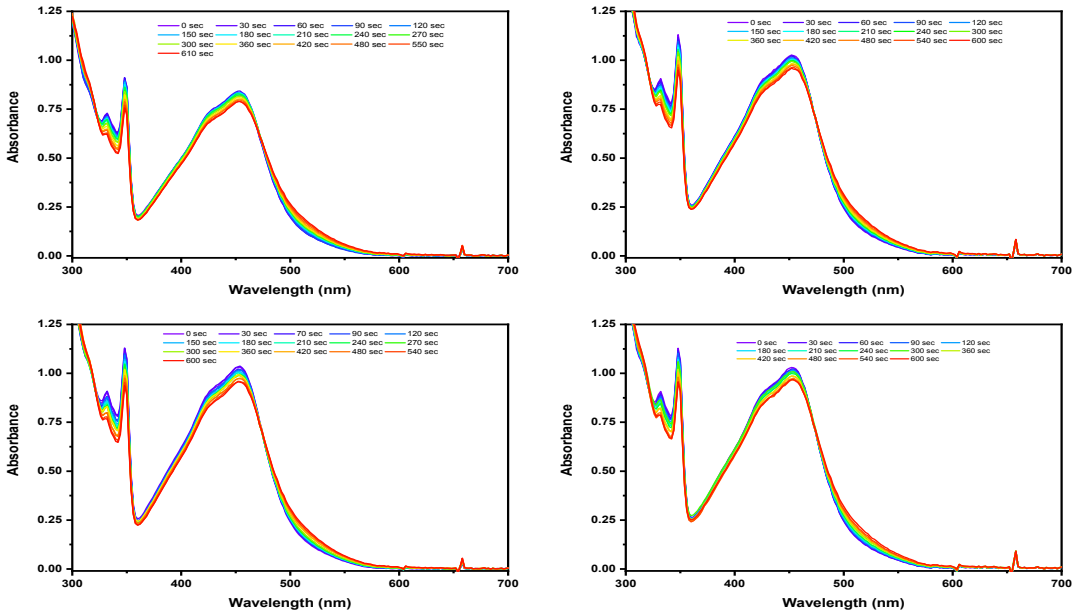


Figure S20. Four repetitions of photolysis of $\mathbf{2^{OMe}}$, monitored by UV-vis spectroscopy.

For calculation of the quantum yield, the concentration of photoproduct was determined from the change in absorbance at 450 nm. This value was then used to calculate the moles of photoproduct generated.

$$A_{450nm} = 15066\ M^{-1}cm^{-1} \times 1\ cm \times [R]$$

$$\Delta A_{450nm} = A_0 - A_t = 15066 M^{-1}cm^{-1} \times 1cm \times [P]$$

$$moles\ of\ photoproduct = [P] * 0.002\ L$$

The moles of photons absorbed by the complex were calculated from the fraction of light absorbed, $F$, by the initial solution, taken from the absorbance at 450 nm, and the photon flux, $Nhv$, calculated by actinometry.

$$A_{450\ nm} = \log 1/T$$

$$T = \frac{1}{10^A}$$

$$F = 1 - T$$

$$moles\ of\ photons\ absorbed = Nhv \times F \times t$$

The quantum yield was then calculated from the following equation:

$$\phi = moles\ of\ photoproduct \div moles\ of\ photons\ absorbed$$

The following table contains the parameters used to calculate each quantum yield for the four iterations:

Table S7.

| Iteration | $A_{450\ nm}$ @ 0 sec | $A_{450nm}$ @ 600 sec | $\Delta A_{450\ nm}$ | [P] (M) | Vol. Irradiated (L) | Moles of P | Fraction of Light Absorbed | Photon Flux (moles hν/min) | Quantum Yield, φ |
|---|---|---|---|---|---|---|---|---|---|
| 1 | 0.82786 | 0.78341 | 0.04445 | 2.95065E-6 | 0.002 | 5.90129E-9 | 0.85136 | 3.92878E-8 | 0.017982 |
| 2 | 1.02106 | 0.95 | 0.07107 | 4.71693E-6 | 0.002 | 9.43386E-9 | 0.90473 | 3.92878E-8 | 0.026541 |
| 3 | 1.02824 | 0.95129 | 0.07695 | 5.10734E-6 | 0.002 | 1.02147E-8 | 0.9063 | 3.92878E-8 | 0.028688 |
| 4 | 1.0255 | 0.96211 | 0.06338 | 4.20706E-6 | 0.002 | 8.41413E-9 | 0.9057 | 3.92878E-8 | 0.023646 |

Based on the quantum yields calculated for the four iterations of this experiment, the average at the 95% confidence interval is 0.0242 ± 0.0064.

**$\mathbf{3}^{\mathbf{OMe}}$:**

As with the samples above, the molar absorptivity at 450 nm was calculated from an absorbance vs. concentration plot.

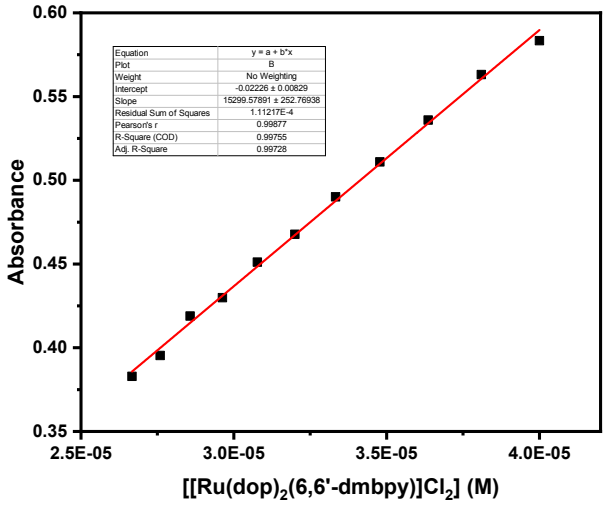


Figure S21. Molar absorptivity determination of $\mathbf{3}^{\mathbf{OMe}}$ at 450 nm.

The molar absorptivity for $\mathbf{3}^{\mathbf{OMe}}$ was calculated to be 15,299 $M^{-1}cm^{-1}$ at 450 nm.

A sample was prepared using the same buffer system as described above and irradiated for a total of 30 minutes, yielding the following absorbance changes over the length of photolysis.

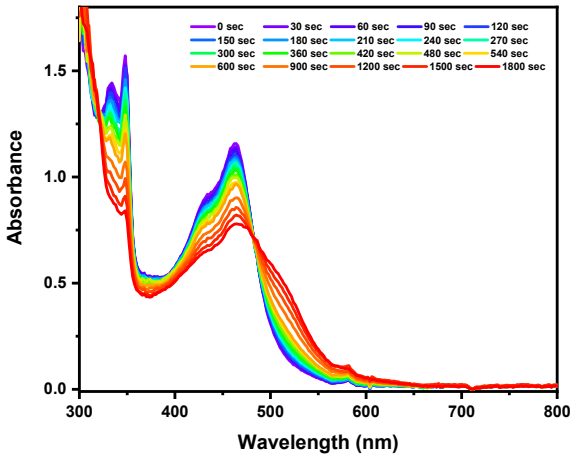


Figure S22. Photolysis of **3**$^{OMe}$ over 30 minutes in buffered phosphate solution.

Photolysis was repeated a total of four times, the spectra are displayed below.

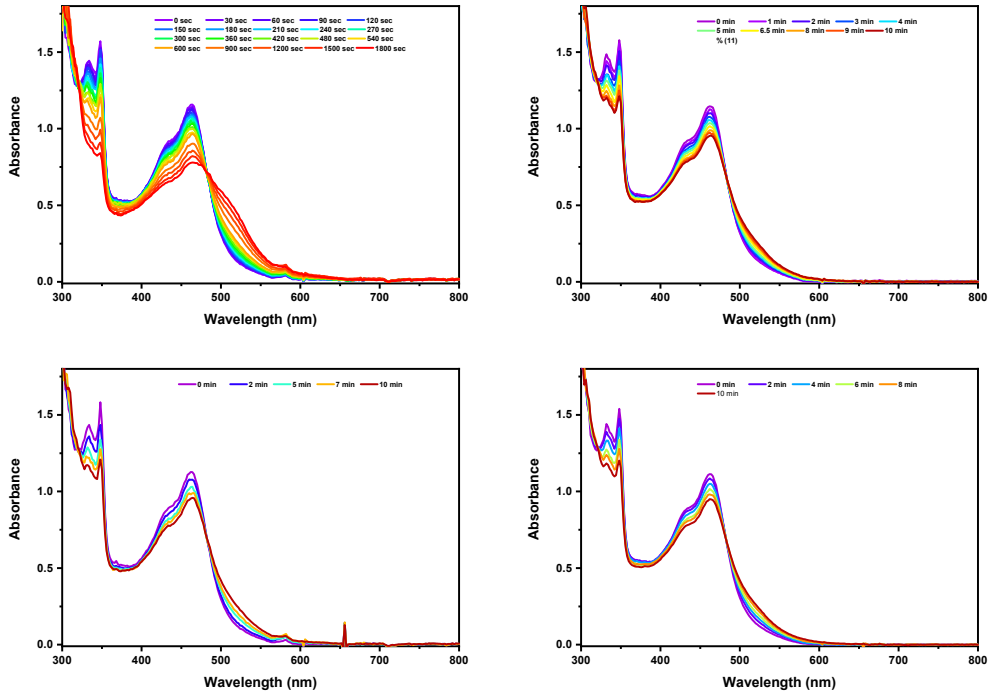


Figure S23. Four repetitions of photolysis of **3**$^{OMe}$, monitored by UV-vis spectroscopy.

The quantum yield was calculated based on the observed changes in the absorption spectra above. The table below includes the relevant data used to compute the quantum yield. The resulting quantum yield

was calculated in the same way as the above two complexes. The quantum yield at the 95% confidence interval was determined to be 3.03E-03 ± 2.3E-04.

Table S8.

| Iteration | $A_{450\ nm}$ @ 0 sec | $A_{450nm}$ @ 600 sec | $\Delta A_{450\ nm}$ | Moles of Product Formed (2 mL volume irr.) | Fraction of Light Absorbed | Photon Flux (moles hν/min) | Moles of Photons Absorbed | Quantum Yield, φ |
|---|---|---|---|---|---|---|---|---|
| **1** | 1.02168 | 0.86716 | 0.15453 | 2.01994E-8 | 0.90487 | 7.06E-7 | 6.38838E-6 | 0.00316 |
| **2** | 1.01797 | 0.8647 | 0.15327 | 2.00358E-8 | 0.90405 | 7.06E-7 | 6.38262E-6 | 0.00314 |
| **3** | 1.00089 | 0.85282 | 0.14807 | 1.93556E-8 | 0.90021 | 7.06E-7 | 6.35545E-6 | 0.00305 |
| **4** | 0.9875 | 0.85228 | 0.13522 | 1.76754E-8 | 0.89708 | 7.06E-7 | 6.33338E-6 | 0.00279 |

**$4^{OH}$:**

Measurements for the quantum yield of $\mathbf{4^{OH}}$ were repeated in the same fashion as above. A new lamp was used as the light source for irradiation and the photon flux was measured as outlined above, yielding a value of 7.06E-7 moles of photons/minute.

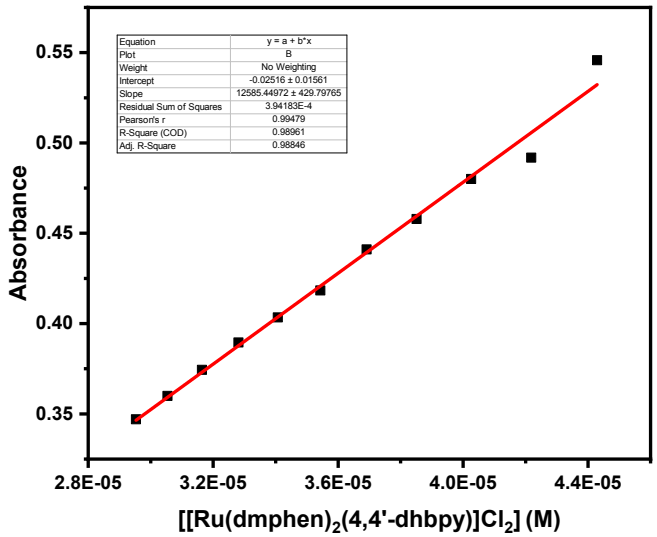


Figure S24. Molar absorptivity determination of $\mathbf{4^{OH}}$ at 450 nm.

The molar absorptivity of the complex, $\mathbf{4^{OH}}$, was obtained at 450 nm. The linear plot of absorbance with concentration is shown above. The molar absorptivity was determined to be 12,585 $M^{-1}cm^{-1}$.

A sample was irradiated over a period of one hour. The results are displayed in the spectrum below. It is clear that a net photolysis product is forming within this time frame.

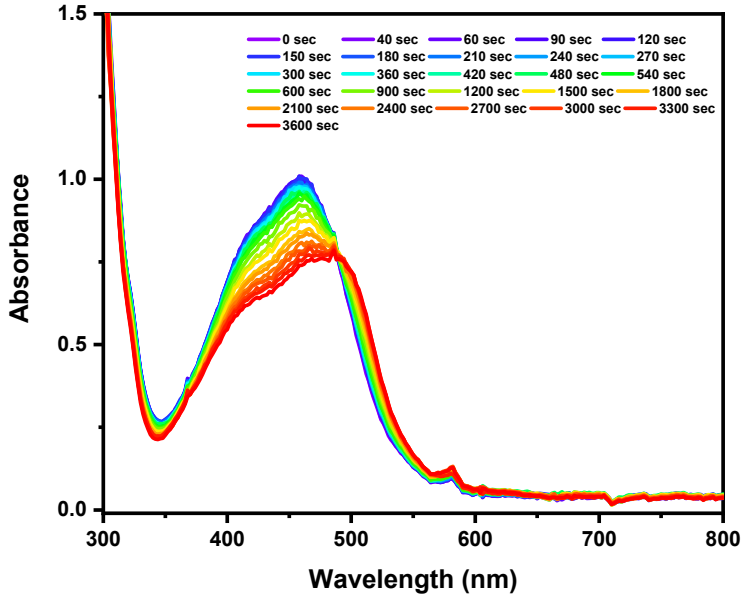


Figure S25. Photolysis of $\mathbf{4}^{\mathbf{OH}}$ over 1 hr in buffered phosphate solution.

Photolysis was repeated a total of 4 times using a fresh sample each time. The spectra are shown below.

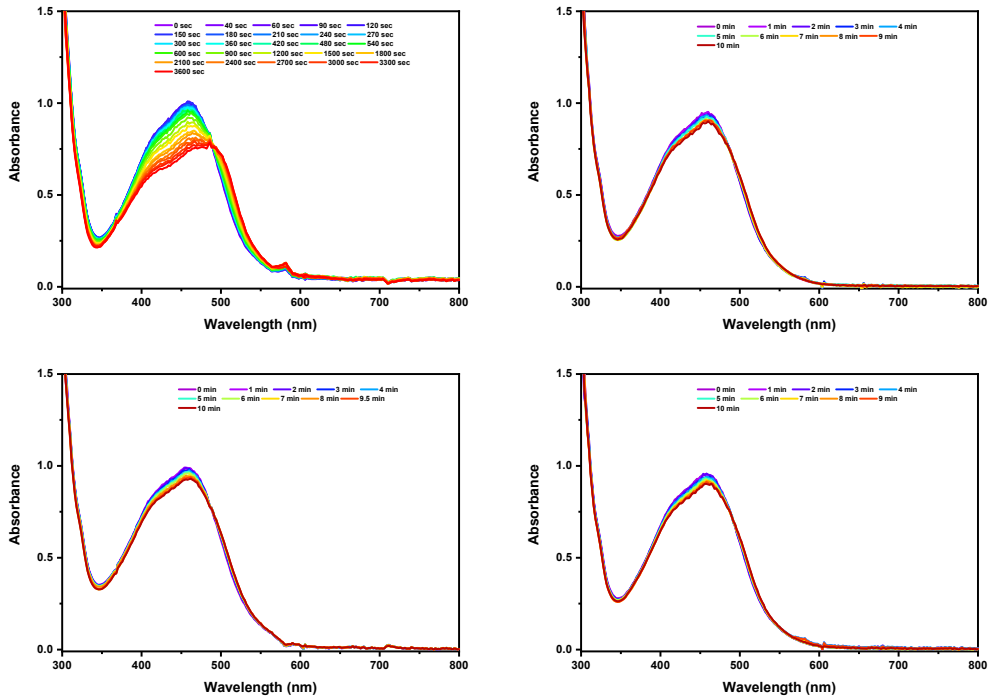


Figure S26. Four repetitions of photolysis of $\mathbf{4}^{\mathbf{OH}}$, monitored by UV-vis spectroscopy.

The quantum yield was calculated using the same rational as for $\mathbf{2}^{\mathbf{OMe}}$. The following table shows the relevant data obtained from the absorbance spectra above.

Table S9.

| Iteration | $A_{450\ nm}$ @ 0 sec | $A_{450nm}$ @ 600 sec | $\Delta A_{450\ nm}$ | Moles of Product Formed (2 mL volume irr.) | Fraction of Light Absorbed | Photon Flux (moles hν/min) | Moles of Photons Absorbed | Quantum Yield, φ |
|---|---|---|---|---|---|---|---|---|
| **1** | 0.96848 | 0.91583 | 0.05264 | 8.36596E-9 | 0.89247 | 7.06E-7 | 6.30085E-6 | 1.328E-03 |
| **2** | 0.92609 | 0.86716 | 0.05893 | 9.36503E-9 | 0.88145 | 7.06E-7 | 6.22301E-6 | 1.505E-03 |
| **3** | 0.96425 | 0.91292 | 0.05133 | 8.15742E-9 | 0.89142 | 7.06E-7 | 6.29342E-6 | 1.296E-03 |
| **4** | 0.94093 | 0.88147 | 0.05946 | 9.4499E-9 | 0.88543 | 7.06E-7 | 6.25114E-6 | 1.512E-03 |

The quantum yield calculated at the 95% confidence interval is 1.41E-03 ± 1.6E-04.

## IX. X-ray structure determinations of $2^{OMe}$ and $4^{OH}$.

Crystals of appropriate dimension were mounted on Mitegen cryoloops in a random orientation. Preliminary examination and data collection were performed on a Bruker Apex2 CCD-based X-ray diffractometer[1] equipped with an Oxford N-Helix Cryosystem low temperature and a fine focus Mo-target X-ray tube ($\lambda$ = 0.71073 Å) operated at 1500 W power (50 kV, 30 mA). The X-ray intensities were measured at 223 (2) K. The collected frames were integrated with the Saint[2] software using a narrow-frame algorithm. Data were corrected for absorption effects using the multi-scan method in SADABS. The space groups were assigned using XPREP of the Bruker ShelXTL[3] package, solved with ShelXT[3] and refined with ShelXL[3] and the graphical interface ShelXle[4]. All non-hydrogen atoms were refined anisotropically. H atoms attached to carbon were positioned geometrically and constrained to ride on their parent atoms. Specific structure determination details are included in Table S11.

The structure of $\mathbf{4^{OH}}$ was found to contain several regions of residual density. Attempts to model the remaining residual density were not successful, so the residual density was "SQUEEZED" (i.e., applied a "solvent mask") out using the PLATON program.[6] The solvent accessible volume was found to be 520 $Å^3$. The electrons found in solvent accessible void is 135 $e^-$, which corresponds to approximately 5 ethanol molecules per asymmetric unit. Hydroxyl H atom positions were restrained based on hydrogen bonding considerations (DFIX and DANG).

Table S10 – Selected metric parameters for crystal structures **$2^{OMe}$ and $4^{OH}$**.

| | Complex $4^{OH}$ | Complex $2^{OMe}$ |
|---|---|---|
| **Crystal data** | | |
| Chemical formula | $[C_{38}H_{32}N_6O_2Ru]Cl_2$ | $C_{36}H_{28}N_6O_2Ru \cdot C_2H_3N \cdot 2(Cl) \cdot H_2O$ |
| $M_r$ | 776.66 | 807.68 |
| Space group | Monoclinic, *P*-1 | Monoclinic, $P2_1/n$ |
| Temperature (K) | 223(2) | 223 (2) |
| Unit cell dimensions | a = 11.3144 (6) Å<br>b = 12.0995 (6) Å<br>c = 15.7429 (8) Å<br>α = 91.563(3)°<br>β = 97.122(3)°<br>γ = 107.140(3)° | a = 10.1716(4) Å<br>b = 20.3819(9) Å<br>c = 16.9731(7) Å<br>α = 90 °<br>β = 91.121(2)°<br>γ = 90 ° |
| $V$ (Å$^3$) | 2038.94 (18) | 3518.1 (3) |
| $Z$ | 2 | 4 |
| Radiation type | Mo $K\alpha$ | Mo $K\alpha$ |
| μ (mm$^{-1}$) | 0.55 | 0.65 |
| Crystal size (mm) | 0.11 × 0.10 × 0.04 | 0.40 × 0.20 × 0.20 |
| **Data collection** | | |
| Diffractometer | AXS *SMARTAPEX2* CCD | AXS *SMART APEX2* CCD |
| Absorption corr. | Multi-scan<br>SADABS | Multi-scan<br>SADABS |
| $T_{min}$, $T_{max}$ | 0.693, 0.746 | 0.0.664, 0.0.746 |
| No. of measured, independent and observed [$I > 2\sigma(I)$] reflections | 60769<br>9012<br>7602 | 143009<br>11574<br>10207 |
| $R_{int}$ | 0.056 | 0.028 |
| $(\sin \theta/\lambda)_{max}$ (Å$^{-1}$) | 0.641 | 0.739 |
| **Refinement** | | |
| $R[F^2 > 2\sigma(F^2)]$<br>$wR(F^2)$<br>$S$ | 0.038<br>0.098<br>1.05 | 0.025<br>0.068<br>1.04 |
| No. of reflections | 9012 | 11574 |
| No. of parameters | 466 | 471 |
| No. of restraints | 2 | 0 |
| H-atom treatment | constrained | constrained |
| $\Delta\rho_{max}$, $\Delta\rho_{min}$ (e Å$^{-3}$) | 0.84, −0.59 | 0.52, −0.46 |

## X. Reference.


(1) Bruker *Apex2*, Apex2 2013.10-0; Bruker AXS Inc.: Madison, Wisconsin, USA, 2007.

(2) Bruker *Saint Plus*, Saint Plus 8.34A; Bruker AXS Inc.: Madison, Wisconsin, USA, 2007.

(3) Sheldrick, G. M. *Acta Cryst.* **2008**, *A64*, 112.

(4) Hübschle, C. B.; Sheldrick, G. M.; Dittrich, B. *J. Appl. Cryst.* **2011**, *44*, 1281.

(5) (a) Sheldrick, G. M. *Acta Cryst.* **2008**, *A64*, 112; (b) Dolomanov, O. V.; Bourhis, L. J.; Gildea, R. J.; Howard, J. A. K.; Puschmann, H. *J. Appl. Crystallogr.* **2009**, *42*, 339; (c) Sheldrick, G. M. *Acta Cryst.* **2015**, *A71*, 3.

(6) Spek, A. L. *Acta crystallographica. Section D, Biological crystallography* **2009**, *65*, 148.